JOURNAL OF MATERIALS SCIENCE 28 (1993) 6365–6370

Damage-tolerant laminated composites in thermal shock

Z. CHEN, J. J. MECHOLSKY JR
Department of Materials Science and Engineering, University of Florida, Gainesville, FL 32611-2066, USA

Alumina is very susceptible to thermal shock which often leads to catastrophic failure. The addition of tape-cast nickel layers to laminated alumina can increase its tolerance to damage induced during thermal shock.The fracture behaviour after thermal shock of laminated composites showed non-catastrophic failure during loading at room temperature. The retained strength of the laminates was determined for a wide range of quenching-temperature differences ($\Delta T = 150$–$1200\,^{\circ}C$). The retained strength and critical quenching-temperature difference, ΔT_c, of the laminated composites were a significant improvement over the values for the respective monolithic alumina. This improvement in behaviour can be related to the compressive residual stress in the alumina layers and ductile-layer crack blunting.

1. Thermal shock resistances of ceramics

Alumina stands out because of its beneficial properties such as high wear/chemical resistance and high temperature retained strength, etc. However, the large statistical spread of its strength due to low toughness and low thermal-shock resistance are the main factors limiting its engineering applications. Many studies have shown several ways of toughening alumina, for example, by second-phase dispersions and phase-tranformation toughening [1, 2]. A previous investigation [3] showed that monolithic alumina could also be toughened and strengthened via the residual compressive stress in the alumina layers and crack blunting by ductile layers. The residual compression and the crack blunting were optimized by strategic location of the nickel layers in alumina laminates. The study also showed that the strength was relatively insensitive to the flaw size. Since most applications invariably involve rapid environmental temperature variations and a high heat transfer, it is important to investigate the thermal-shock resistance of the laminated composites.

In general, fracture-initiation resistance and (catastrophic) crack-propagation resistance are the two design principles used to select thermal-shock resistant ceramics. For fracture-initiation resistance, the capacity is described by [4, 5]

$$R^{I} = \frac{k(1-\nu)\sigma_t}{E\alpha} \quad (1)$$

where R^I is the thermal shock resistance, σ_t, is the strength, E is the elastic modulus, ν is Poisson's ratio, k is the thermal conductivity, and α is the linear thermal-expansion coefficient. In order to achieve high resistance, a high strength and thermal conductivity and a relatively low elastic modulus and thermal expansion coefficient are required. When cracks are initiated during thermal shock, the resistance to catastrophic crack propagation, R^{II}, is evaluated by [4, 5]

$$R^{II} = \frac{EW_c}{\sigma_t^2(1-\nu)} \quad (2)$$

where W_c is the work of fracture. For high R^{II} resistance, the ratio of the work of fracture and the elastic modulus over the strength must be maximized. For most materials, it is difficult to satisfy the requirement of maximizing both R^I and R^{II} because of contrasting requirements in Equations 1 and 2. However, if the work of fracture of materials is significantly increased, that is, if the ratio of EW_c/σ_t^2 increases even for a high value of σ_t and a low value of E, then maximizing both resistances can be achieved. This paper investigates the thermal-shock capacity of alumina/nickel-laminated composites and incorporates the residual-compressive-stress influence of crack initiation in the alumina layers and the ductile-layer-crack-blunting influence of crack propagation in the alumina layers after thermal shock (ΔT greater than the critical-quenching-temperature difference, ΔT_c, of monolithic alumina).

2. Thermal shock-testing experimental procedure

Thermal-shock experiments were performed by measuring the retained bending indent strength after quenching specimens from successively higher temperatures in water at 28 °C. An indentation technique was used to induce controlled cracks before quenching in order to control the fracture of quenched specimens. This technique was used because, for most brittle ceramics, the fracture is likely to be strongly affected by the flaws created during processing and sample preparation, and reliance on this kind of strength measurement to measure thermal-shock resistance, that is, the critical-quenching-temperature difference,

0022–2461

TABLE I Specimen designation, strength, work of fracture, thermal-crack-initiating resistance, and thermal-crack-propagating resistance

Sample Designation[a]	Thichness (Ni, mm)	Thickness (Al_2O_3, mm)	Strength (MPa)	W_c (kJm^{-2})	R^I (kW)	R^{II} (mm)
LC180	180	320	732 ± 22	1.72	5.36	1.62
Al_2O_3		2000	556 ± 45	0.07	3.86	0.12

[a]LC180 is alumina/nickel-laminated composite, Al_2O_3 is monolithic alumina.
The thickness of the outside alumina layers was about 200 μm.

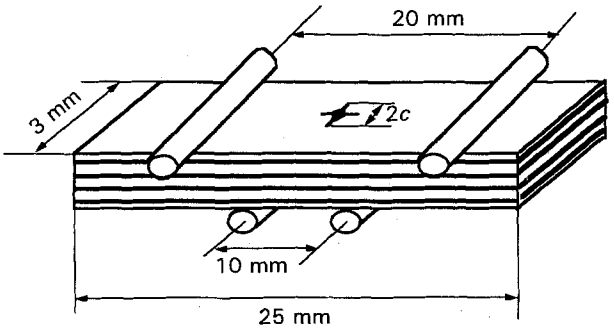

Figure 1 Schematic illustration of the specimen used for retained-strength measurements. $2c$ = 421 μm and 343 μm for monolithic alumina and the laminated composite, respectively.

ΔT_c, is unlikely to give any insights. Pre-cracking of the specimen surface was performed using a 117.6 N load with a Vickers diamond indenter. Monolithic-alumina and alumina/nickel-laminated composite samples were prepared by tape casting followed by hot pressing. Details of the processing of the laminated composites are described elsewhere [3].

Four-point flexure specimens (see Fig. 1) with dimensions of 25 mm (length), 3 mm (width), and about 2.0 mm (thickness) were broken using a tensile-testing machine (Model 1125, Instron Corporation, 100 Royall Street, Canton, Massachusetts 02021, USA) with spans of 20/10 mm at a crosshead rate of 0.0085 mm s^{-1} after thermal shock (ΔT = 150–1200 °C). The load–displacement curves were recorded. The strengths, (σ_t), and indent strength of monolithic alumina and the alumina for the laminated composites were calculated using mechanics and classical laminated-plate theory [6], respectively. The work of fracture of monolithic alumina and the laminated-composite specimens with a 147 N Vickers indentation load was computed using

$$W_c = \int_0^{e^*} \frac{F(e)}{A}\,de \qquad (3)$$

where $F(e)$ is the load, e^* is a displacement at the point of fracture through the whole cross-section, A is the projected fracture area, and e is the displacement.

3. Thermal-shock resistant capacity of the composite

The strength, σ_t, and the work of fracture, W_c, of both monolithic alumina and the laminated composite were calculated and are listed in Table I. Since the alumina layers in the laminated composite were assumed to retain the same composition and structure as the monolithic alumina, their elastic modulus

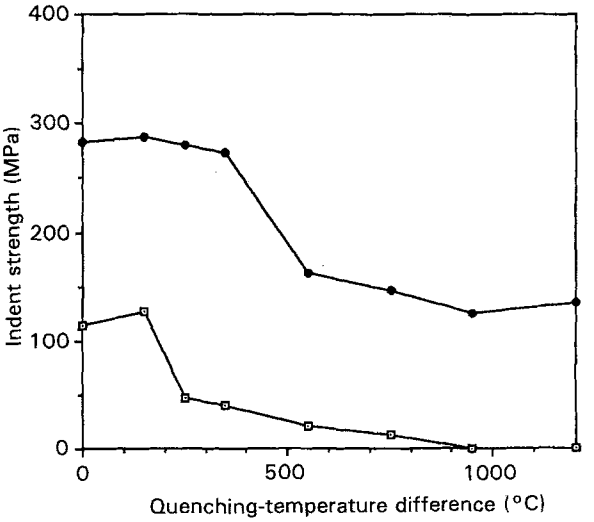

Figure 2 Retained indentation strength after thermal shock as a function of the quenching-temperature difference. The retained strength shows an increase in thermal-shock resistance of the laminated composites over that of the monolithic alumina: (●) laminated conposite, and (⊡) monolithic alumina.

(E = 380 GPa), thermal conductivity (k = 0.29 W cm^{-1} °C^{-1}) and thermal-expansion coefficient ($\alpha = 8.237 \times 10^{-6}$ °C^{-1}) were assumed to be the same as those of monolithic alumina. These parameters were put into Equations 1 and 2, and the resistances to thermal-shock crack initiation, R^I and crack propagation, R^{II} were computed and are shown in Table I. Both R^I and R^{II} for the laminated composites were significant improvements on the values for the monolithic alumina. Thus, the retained strength and the value of ΔT_c after thermal shock of the laminated composite should be an increase over the values for the monolithic alumina.

The retained strength after thermal shock of monolithic alumina and of the laminated composite were determined for a wide range of quenching-temperature differences (ΔT = 150–1200 °C), and strength-degradation curves are plotted in Fig 2. The monolithic alumina exhibited a rapid reduction in strength at ΔT_c = 250 °C (about 40% of the strength of non-thermal-shocked alumina). This reduction implies that the cracks in alumina begin to be propagated by thermal shock at $\Delta T > \Delta T_c$. When ΔT exceeds 950 °C, the monolithic alumina cracks into several pieces and has no measurable retained strength. Its resistance to crack propagation seems to be low, and catastrophic failure occurs when the monolithic alumina specimen has a large thermal-strain energy (a large ΔT).

When nickel layers are placed in strategic locations in the alumina laminate, the alumina's retained

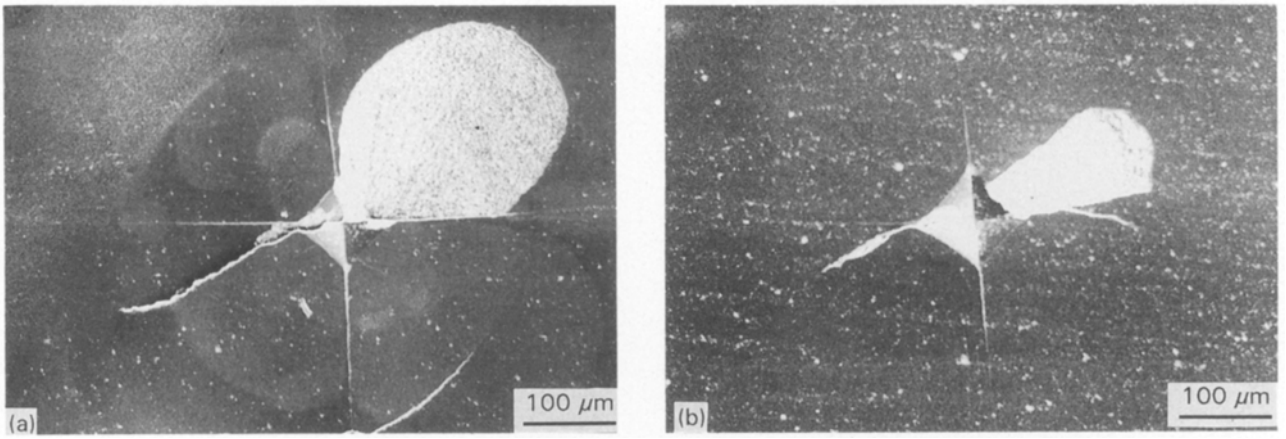

Figure 3 Scanning electron microscopy (SEM) graphs of indentation cracks after thermal shock: (a) monolithic alumina, and (b) laminated composite. The indent radial cracks on the laminated composite did not extend after a $\Delta T = 350\,^{\circ}C$ thermal shock; compare with monolithic alumina, in which the cracks did extend. This indicates that the ΔT_c of the composite increased.

strength after thermal shock of the composite is as high as twice that of the monolithic alumina (Fig. 2). The retained strength decreased about 30% when ΔT exceeded 350 °C compared with the strength of non-thermal-shock laminated composites. After that, the strength degradation progresses slowly to a ΔT of about 550 °C; thereafter, the retained strength remains almost unchanged at about 120 MPa. Fig. 3 shows indentation cracks on the surface of both monolithic alumina and the composite at a $\Delta T = 350\,^{\circ}C$ thermal shock. The radial cracks on the monolithic alumina specimen extended approximately twice as far as they did before the thermal shock. The radial crack before the thermal shock was $2c = 421\ \mu m$. Thermal shock caused the retained indent strength to drop by a relatively large amount (> 40%). For the laminated composite, the radial cracks did not extend and remained the same as before thermal shock. The radial crack in the laminated composites before the thermal shock was $2c = 343\ \mu m$. The indent strength of the composite seems not to be affected by the thermal shock at this ΔT level. When ΔT exceeds 350 °C, the indentation cracks on the composite start to extend. Fig. 4 shows thermally induced radial cracks on both monolithic alumina and the composite after a $\Delta T = 550\,^{\circ}C$ and 1200 °C thermal shock, respectively. Even though thermal cracks began to initiate or propagate in the composite specimens, the situation seems to be much less severe when compared with thermal cracks in the monolithic–alumina specimens. No cracking in the composite specimens was observed even under a severe $\Delta T = 1200\,^{\circ}C$ thermal shock. No delamination was observed even after wide ranges of temperature differentials in the thermal shock. However, delamination is often observed along the interface in many ceramic/metal systems [7, 8]. The behaviour of the present composites indicates that a very good bond can be formed between alumina and nickel using tape casting followed by hot pressing.

Fig. 5 shows a side view of the composite specimen which experienced a $\Delta T = 1200\,^{\circ}C$ thermal shock. Fig. 5 shows many cracks in the alumina layers which were caused by a large amount of thermal-strain energy. However, the ductile layers which resulted in higher R^{II} values in the composite stopped catastrophic crack propagation through the cross-section and the residual compressive stress left the composite with a retained strength of about 120 MPa. Unlike the composite, when the thermal-strain energy reaches such a large amount in monolithic alumina, the thermally induced cracks propagate through the cross-section of the samples and cause the specimen to fracture in several pieces.

The increase of resistance to thermally induced crack propagation is attributed to nickel-layer crack blunting in the composite. The high-magnification scanning electron microscopy (SEM) micrograph in Fig. 5b shows that a crack was blunted and arrested by the nickel layer at the interface. Fig. 5b is also evidence that a good bond between alumina and nickel still exists in the composite after the specimen had a severe thermal shock ($\Delta T = 1200\,^{\circ}C$). Load–displacement curves (Fig. 6) show a decrease in the stiffness of the composite but an increase in its plastic behaviour when ΔT exceeds 350 °C. This toughening of the composite was attributed to the amount of thermally induced cracks initiated in the alumina layer and blunted at the interfaces by the nickel layers during high-thermal-strain-energy thermal shocks.

Fracture-path analysis reveals that the thermally induced cracks were blunted and arrested by ductile layers, and the ductility of nickel layers absorbed significant amounts of fracture energy by local plastic deformation (Fig. 5b). The behaviour of the ductile layers contributes to an increase in the amount of resistance to thermally induced crack propagation. Further study focused on the cause of the increase to resistance of thermally induced crack initiation, R^{I}, in the composite. The previous paragraph showed that the critical-quenching-temperature difference, ΔT_c, of the composite increases above 100 °C over that of monolithic alumina. From Equation 1, an increase in R^{I} is attributed to an increase in the strength of the alumina, σ_i, because E, k and α values of the alumina in the composite are assumed to be the same as those in monolithic alumina. Therefore, the increase in strength is attributed to a residual compressive stress

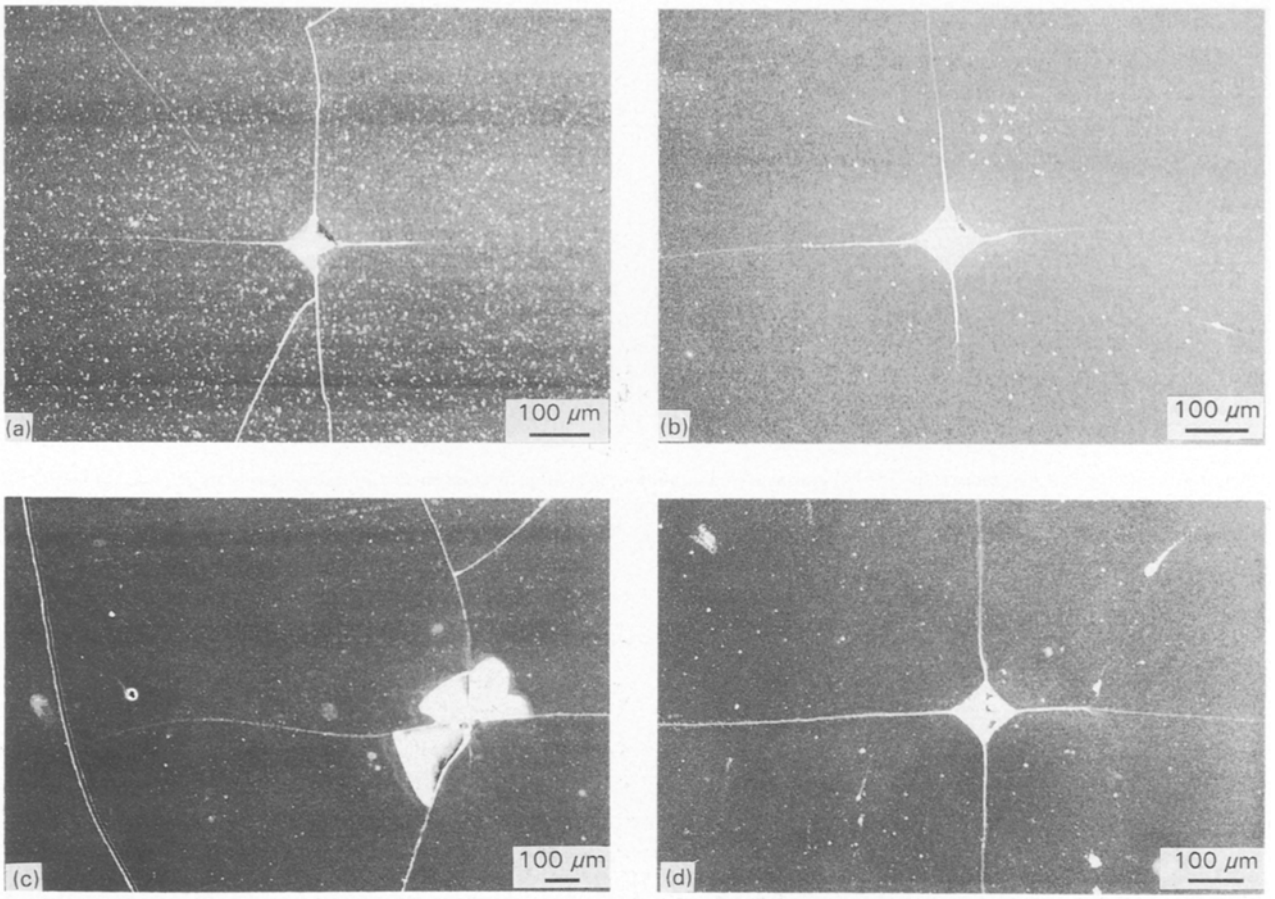

Figure 4 SEM micrographs of indentation cracks after thermal shock: (a) 550 °C, monolithic alumina; and (b) 550 °C, laminated composite; (c) 1200 °C, monolithic alumina; and (d) 1200 °C, laminated composite. Less severe damage was caused by different ΔT thermal-shock conditions in the laminated composite than in the monolithic alumina.

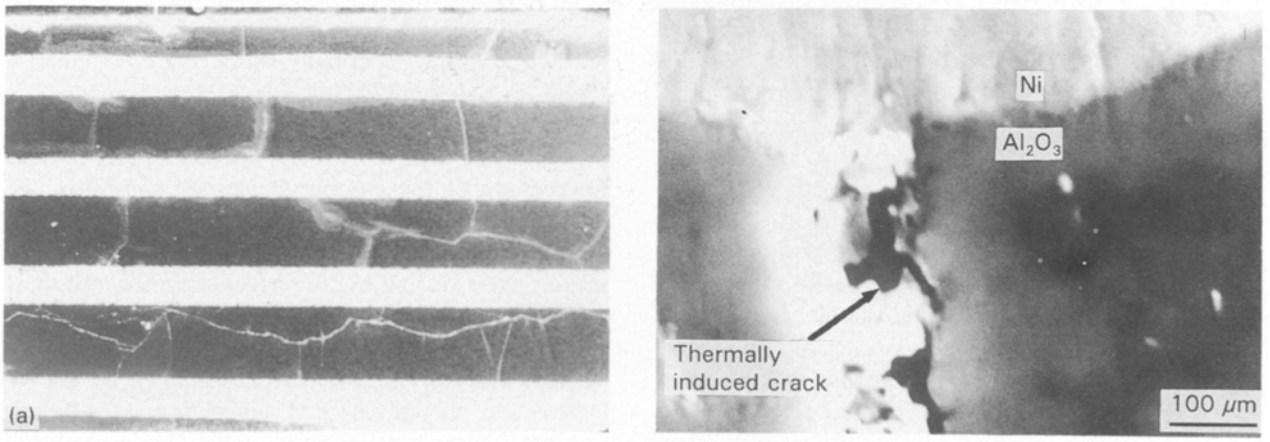

Figure 5 (a) Low and (b) high-magnification SEM micrographs of cracks in a laminated composite after thermal shock. Thermal cracks were stopped (blunted) by ductile layers in the laminated composite after a $\Delta T = 1200$ °C thermal shock, which illustrated that high resistance to thermal-crack propagation was achieved. In (b) there is no delamination after the severe thermal shock.

in the alumina layers due to the thermal-expansion-coefficient mismatch between the alumina and nickel layers. The residual compressive stress in the alumina layers was determined using an indentation technique.

The existence of residual compression in the alumina layers can be demonstrated by observation of the change in the length of the radial cracks induced by a Vickers indenter. Vickers indentations were placed in the alumina layers. In the absence of residual stress, the length of the cracks, c, emanating from the adjacent corner of the impressions should be almost equal, due to a uniform stress field. When a residual stress field exists in the alumina layers, the length of radial cracks, c^*, normal to the residual compression is prevented from growing and can be related [9,10] to the magnitude of the residual stress, σ_r by

$$\sigma_r = \frac{K_c - [\eta(E/H)^{1/2}P(c^*)^{-3/2}]}{\Omega\,(c^*)^{1/2}} \qquad (4)$$

where Ω is a coefficient related to the residual stress

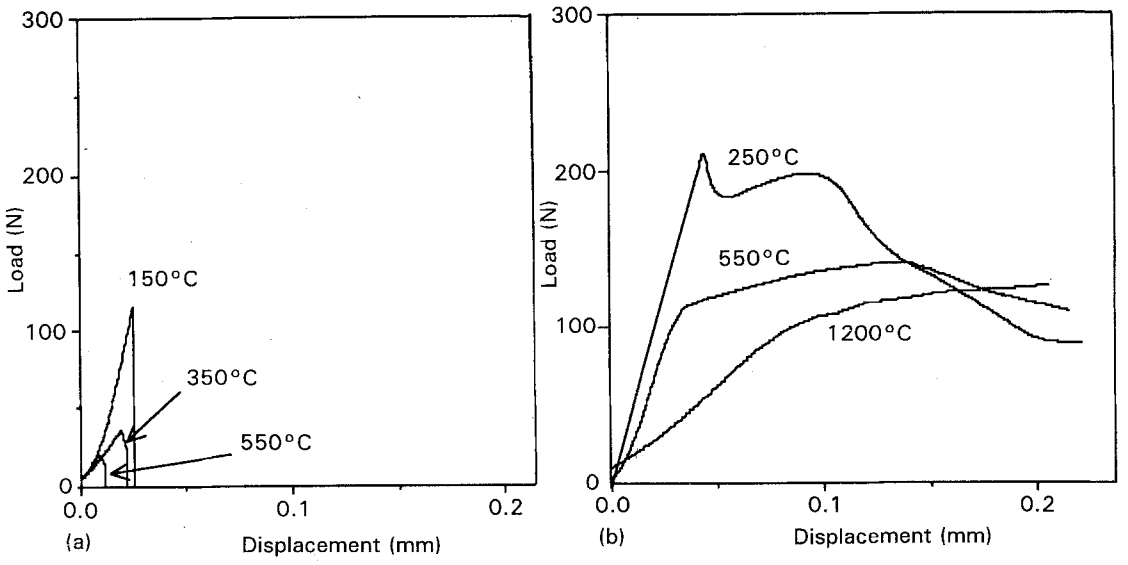

Figure 6 Load–displacement curves after thermal shock of: (a) monolithic alumina, and (b) laminated composites. The plastic behaviour of the laminate was a significant improvement on that of the monolithic alumina.

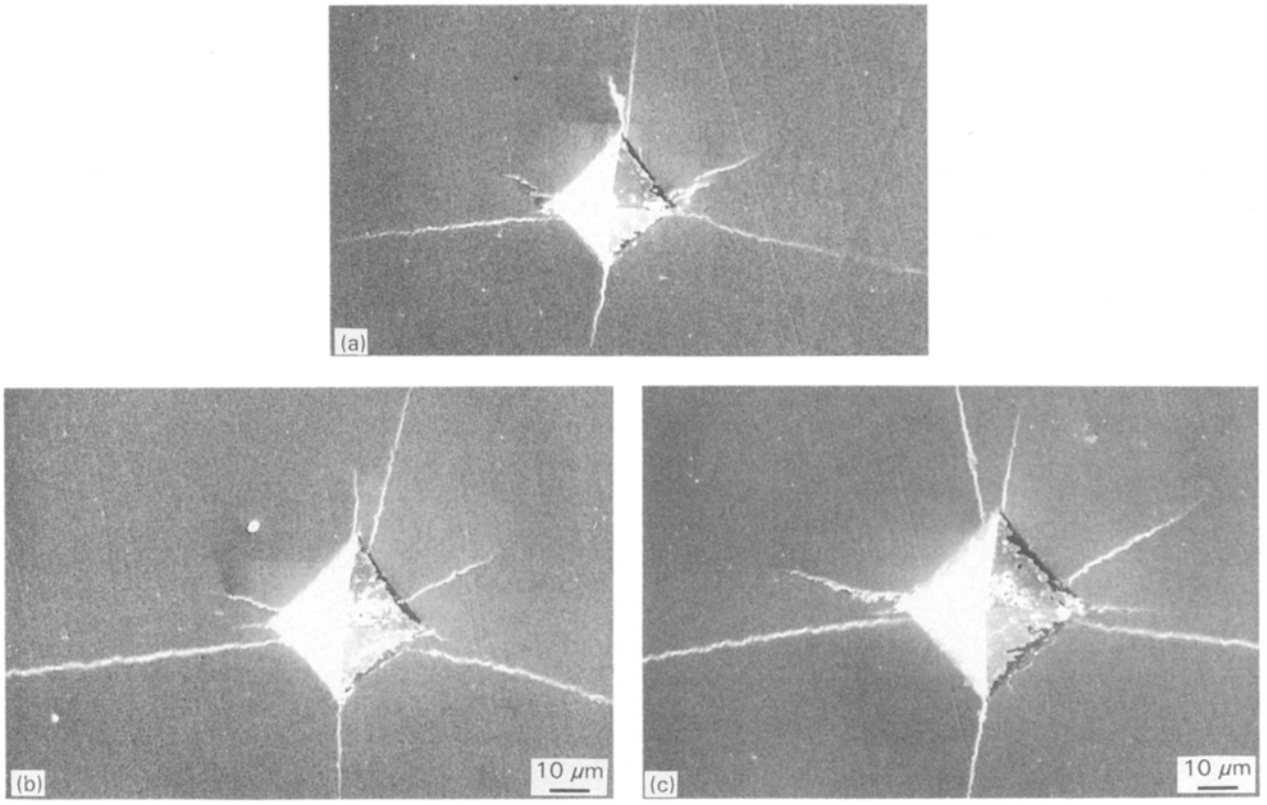

Figure 7 SEM micrographs of indentation cracks in the alumina layers near the alumina/nickel interface (top of the micrographs). The effect of the residual stress on the length of the indentation cracks in the alumina layers is shown for indent loads of: (a) 19.8 N, (b) 29.4 N, and (c) 39.2 N.

field ($\Omega = 2/\pi^{1/2}$ for a uniform residual stress field [10]), η is a material-independent constant for Vickers-produced radial cracks ($\eta = 0.014$ for alumina [11]), K_c is a measure of the toughness ($K_c = 2.8\ \text{MPa m}^{1/2}$)[3] H is the hardness of alumina ($H \simeq 18.2$ dGPa) [3], and P is the indent load. Three different indent loads were selected (19.8, 29.4 and 39.2 N) depending on the convenience for crack measurement and the avoidance of an influence by the interfaces. Fig. 7 shows the radial cracks and Vickers impressions for these three indent loads. The residual stress was calculated using Equation 4 and plotted against the indent load (Fig. 8). The calculations result in about a 110 MPa compressive residual stress in the alumina layers. This 110 MPa compressive stress can account for much of the over 150 MPa retained strength increase and the 100 °C increase in ΔT_c for the laminated composites over the monolithic alumina which was observed in the strength degradation curves of Fig. 2.

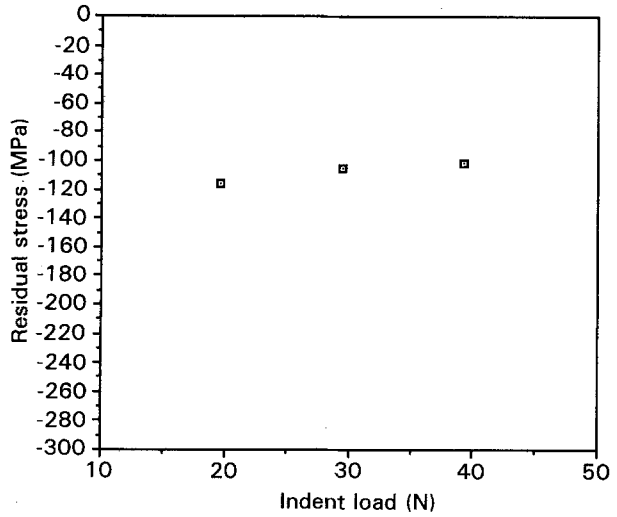

Figure 8 Compressive residual stress versus indent load as described by Equation 4.

There is no evidence showing that the higher thermal conductivity of nickel contributes to the improvement in the thermal-shock resistance capacity of the laminated composites.

4. Conclusions

The thermal-shock behaviour of tape-cast alumina/nickel-laminated composites exhibits some attractive features. The retained strength after thermal shock for a wide range of temperatures (ΔT = 150–1200 °C) was increased by an increment of more than 150 MPa compared to the strength of monolithic alumina corresponding to each ΔT. Moreover, the critical-quenching-temperature difference was enhanced by more than 100 °C over the monolithic alumina (ΔT_c = 250 °C). Non-catastrophic fracture for the laminated composite is desirable for industrial applications. This investigation found that the increase in both the resistance of thermal-crack initiation and crack propagation is attributable to a compressive residual stress existing in the alumina layer and to crack blunting by the nickel layers. This type of laminated composite gives a way of improving the thermal-shock resistance and damage tolerance of ceramics.

References

1. C. O. McHUGH, T. J. WHALEN and M. HUMENIK JR, *J. Amer. Ceram. Soc.* **49** (1966) 486–49.
2. N. CLAUSSEN, *ibid.* **60** (1976) 49–51.
3. Z. CHEN and J. J. MECHOLSKY, *ibid.* **75** (1993) 1258–1264
4. D. P. H. HASSELMAN, *ibid.* **52** (1969) 600–04.
5. J. NAKAYAMA, in "Fracture mechanics of ceramics", Vol. 2, edited by R. C. Bradt, D. P. H. Hasselman and F. F. Large (Plenum Press, New York, London 1974) pp. 759–78.
6. Z. HASHIN and B. W. ROSEN, "Fiber composite analysis and design", Vol. I, (1983), DOT/FAA/CT = 85/6, (Atlantic City Airport, NJ, US Department of Transportation Federal Aviation Administration, 1985) pp. 3-1-148 to 3-108-247.
7. A. BARTLETT and A. G. EVANS, *Acta Metall.* **39** (1991) 1579–85.
8. H. P. KIRCHNER, J. C. CONWAY and A.E. SEGALL, *J. Amer. Ceram. Soc.* **70** (1987) 104–109.
9. P. CHANTIKUL, G. R. ANSTIS, B. R. LAWN and D. B. MARSHALL, *ibid.* **64** (1981) 539–43.
10. C. H. HSUEH and A. C. EVANS, *ibid.* **68** (1985) 120–27.
11. M. REECE and F. GUIU, *ibid.* **74** (1991) 148–54.

Received 5 February
and accepted 24 May 1993